ELSEVIER

1 November 1997

Optics Communications 143 (1997) 42–46

OPTICS COMMUNICATIONS

Compact single-frequency diode-pumped Cr:LiSAF lasers

R. Knappe *, G. Bitz, K.-J. Boller, R. Wallenstein

Fachbereich Physik, Universität Kaiserslautern, 67653 Kaiserslautern, Germany

Received 25 April 1997; accepted 17 June 1997

Abstract

We report on the performance of diode-pumped Cr:LiSAF lasers with coupled optical cavities for single-frequency operation and wavelength tuning. One of these lasers consists of a 500 μm long, highly doped Cr:LiSAF crystal (one surface is HR coated, the other uncoated) and a 0.3% flat output coupler positioned at a distance of 10 μm from the uncoated crystal surface. Pumped by 30 mW of 670 nm diode laser radiation this laser generated single-frequency radiation with a power of 5 mW and a spectral width of 3 MHz at wavelengths within the tuning range of 860 to 900 nm. A second short cavity Cr:LiSAF laser was operated with an external grating resonator. This laser produced a single-frequency output of 16 mW with a linewidth of ~ 1 MHz. The wavelength was tunable in the range of 800–970 nm. The performance of these lasers is analyzed by characterizing the optical cavity (which is determined by the thermally induced changes of the refractive index and the unisotropic thermal expansion of the laser crystal), by integrating the relevant rate equations, and by solving the electric field equations for the coupled cavities. © 1997 Elsevier Science B.V.

Diode laser based tunable single-frequency lasers in the near infrared are of interest for scientific and technical applications [1]. Until now, the Ti:sapphire laser, which operates in the wavelength range from 680 to 1050 nm, has been widely used as a tunable single-frequency source. The operation of this laser requires, however, a green laser as pump source which is disadvantageous for many practical applications. With the recent development of more powerful and reliable high brightness red diode lasers, diode-pumped Cr^{3+}:$LiSrAlF_6$ (Cr:LiSAF) lasers are an interesting alternative. In fact, diode-pumped single-frequency Cr:LiSAF ring lasers have been demonstrated, with high efficiency (20%) [2], a broad tuning range (810–860 nm) [3] and linewidths as narrow as 100 kHz [1]. However, these lasers are still sophisticated devices, which contain many intracavity elements such as Faraday rotators and etalons. These elements are not only costly but reduce the overall efficiency.

An elegant concept for single-frequency lasers is the monolithic microchip design. Such laser devices are small in size and reliable in operation [4]. Narrow linewidths of less than 5 kHz have been demonstrated with microchip lasers of different neodymium- [4] and other rare earth-doped crystals [5]. In addition continuous wavelength tuning has been reported. The output of a Nd:YVO_4 laser was tuned over a range of more than 100 GHz by an appropriate thermal and electro-optical control of the optical cavity length [6].

Compared to rare earth materials, the gain bandwidth of Cr:LiSAF (780–950 nm) is broader by three orders of magnitude. Since single-frequency operation of a microchip laser requires a mode spacing which exceeds the gain–bandwidth, the resonator length of a Cr:LiSAF microchip laser should be about 1 μm, which is clearly impossible.

A resonator concept, well suited for such laser material, is a short monolithic laser-active cavity combined with an additional frequency selective resonator. A Cr:LiSAF laser, based on such concept has been reported by Zhang et al. [7]. The laser was tuned from 850 to 935 nm by using a Lyot filter or a liquid-crystal retarder as frequency selective elements inside the additional cavity. Although single-mode operation was achieved with this device at

* E-mail: knappe@rhrk.uni-kl.de.

PII S0030-4018(97)00330-1

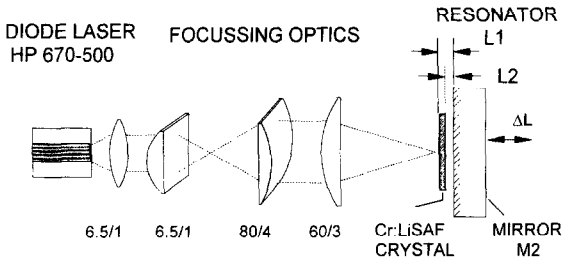

Fig. 1. Setup of the diode-pumped short cavity Cr:LiSAF laser (the numbers indicate the focal length and F-number of each lens).

discrete wavelengths, it suffered from amplitude instabilities. When tuned electronically with the liquid-crystal retarder (from 858 to 920 nm), the laser output was not single frequency, but contained several longitudinal modes.

Stable single-frequency operation was achieved by Sutherland et al. [8] with a Cr:LiSAF laser with a composite cavity consisting of two highly reflective (HR) coated thin crystals separated by a 130 μm quartz spacer. Due to the six intra-cavity surfaces, this device could be tuned to a few discrete wavelengths. The output power was limited to 1 mW.

In our experiments, we combined the stability and the narrow linewidth of a short cavity laser with the wide tunability provided by appropriate coupled cavities. As seen from Fig. 1 the low-loss laser resonator consists of the HR-coated surface of a 500 μm thick, 5.5%-doped Cr:LiSAF crystal (mirror M1) and a flat mirror M2 as output coupler. The crystal coating (HR for 780 to 950 nm) is transmissive ($T = 92\%$) at 670 nm. The second surface of the crystal is uncoated with a residual reflectivity of 3%. The crystal (mounted on a temperature controlled copper heat sink) absorbes 86% of the pump light, transmitted by the coated surface. This corresponds to an absorption coefficient of $\alpha = 22.5\ \mathrm{cm}^{-1}$. Due to the short length, the crystal internal losses are expected to be less than 0.1% per roundtrip. The overall losses of $L = 1.14 \times 10^{-3}$ (which include the losses at the crystal coating) were determined from a Findlay-Clay plot [9].

The pump source is a high-brightness broad-area diode laser (Uniphase HP-067-0500-C, $\lambda = 670$ nm). This diode laser emits a power of 500 mW from a 100 μm wide facet. Because of the long cavity of 1000 μm and the low reflectivity ($< 5\%$) of the front facet [10], this diode laser oscillates in low order transverse modes. The measured M^2 value of the diode laser output is about 15 to 30 (depending on the output power) while typical values for broad area diode lasers are in the range of 40 to 100.

The output of the diode laser was collimated with a lens triplet ($f = 6.5$ mm) in the fast axis, magnified with a cylindrical telescope (1:12) in the slow axis and focused with a spherical lens ($f = 60$ mm) to a beam waist of 13×20 μm.

The optical geometry of the resonator was determined mainly by thermal effects in the crystal. Due to the strong absorption of pump light in a small volume, the crystal was heated at the centre. This causes a strong radial temperature gradient and correspondingly a change of the refractive index and a mechanical expansion of the crystal. The thermally induced gradient of the refractive index is, due to the negative $\mathrm{d}n/\mathrm{d}t$, equivalent to a negative lens. Because of the mechanical expansion, the crystal surfaces are no longer flat but curved in such a way that the concave shape not only compensate the negative thermal lens, but forms an optically stable cavity [11].

Values for the focal length of the thermal lens and the curvature of the crystal surfaces were obtained from numerical analysis. The strong difference of the thermo-optical properties along the different crystal axes excluded the use of a simple analytical model. Using a finite element computer program (MSC/NASTRAN) [12] we calculated

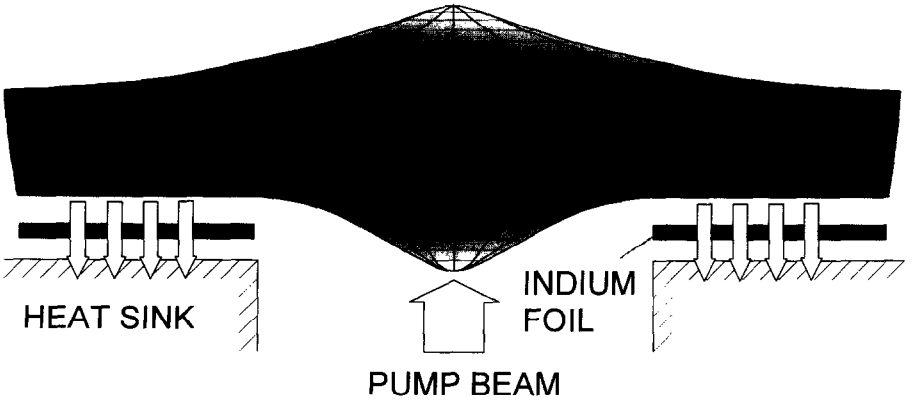

Fig. 2. Mechanical deformation of the 500 μm thick Cr:LiSAF crystal, heated at the center by the focussed pump radiation. The expansion is shown with a vertical magnification of 600. The arrows indicate the heatflow from the crystal to the copper heat sink. An indium foil improves the thermal contact.

a self-consistent three-dimensional thermal distribution inside the crystal determined by the pump power distribution and the boundary conditions. From the temperature distribution we obtained the spatial distribution of the refractive index and the mechanical deformation of the crystal which considers the thermal expansion along the different crystal axes.

A typical example of the mechanical deformation of the crystal (calculated for a pump power of 0.5 W) is shown in Fig. 2. At the pumped surface the temperature difference between the centre of the crystal and the surface area in contact with the heatsink was 100°C. On the opposite surface this difference was 60°C with an exponential decrease in between. As a result, the thermal expansion created a protuberance with a radius of curvature of 14 mm in the central area of the coated crystal surface, and of 30 mm on the opposite surface.

The cavity beam waist was calculated with the usual matrix algorithm. The contribution from the thermally induced lens was taken into account by calculating the change of the refractive index from the temperature profile in the x- and y-directions [13]. Along the optical z-axis, the exponentially decreasing temperature profile was approximated by a step-function. The temperature was averaged in each step. This resulted in a series of matrices, which describe the propagation of the beam along a single pass through the crystal. Due to the negative dn/dt (-2.5×10^{-6} K^{-1} $\perp$ C, -4.0×10^{-6} K^{-1} ||C) [14] the distribution of the refractive index forms a negative lens which reduces the resonators optical stability. However, the curvature of the crystal surfaces, caused by the thermal expansion, was strong enough not only to compensate this lens, but to provide an optically stable resonator.

The calculated waist of the TEM_{00} cavity mode depends, of course, on the absorbed pump power as shown in Fig. 3. As seen from this figure, calculated values are in good agreement with the values, derived from the divergence of the laser beam. It should be noted that the calculations are based only on material constants and did not use any fit parameter. For all applied pump powers the waist of the resonator mode was larger than the pump focus. This resulted in high transverse mode selectivity, and good efficiency. The output beam was Gaussian with an $M^2 < 1.2$.

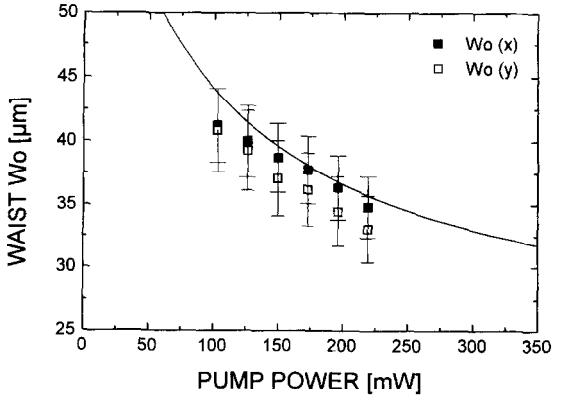

Fig. 3. Waist size of the TEM_{00}-mode of the thermally induced optical resonator, measured as a function of the pump power. The curve represents the data calculated from the thermal change of the refractive index and the crystal's thermal expansion.

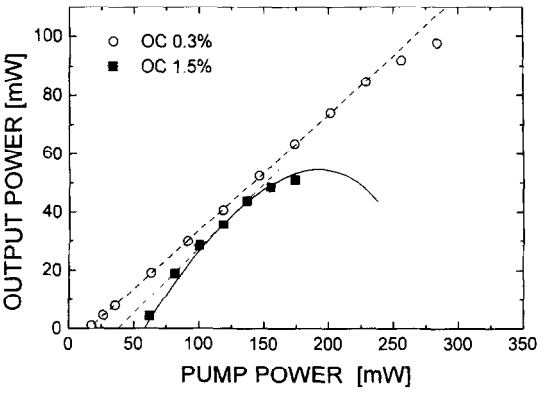

Fig. 4. Output power of the coupled-cavity Cr:LiSAF laser measured for two different output coupler transmissions. The dotted lines represent a linear fit to the experimental data, the solid curve the power predicted by a solution of the appropriate rate equations.

For pump powers of up to 30 mW the laser oscillated in a single longitudinal mode with an output power of 5 mW and a linewidth of 3 MHz. The wavelength was tunable from 860 nm to 900 nm by changing piezoelectrically the length of the small air gap between the laser crystal and the external mirror. By tuning the cavity length in this way the wavelength changed in steps of 0.6 nm, which corresponds to the free spectral range (FSR) of the resonator, formed by the crystal surfaces. Tuning to any desired wavelength was achieved by controlling the width of the air gap and the crystal temperature simultaneously. A change of the crystal temperature by 31°C tuned the laser wavelength by 0.6 nm, the crystals free spectral range.

At higher pump powers the laser oscillated on 5 to 10 longitudinal modes, separated by 0.6 nm, in the range of 860–870 nm. Optimum output power was measured for output coupler (OC) transmissions of 0.3–0.7%. The measured dependence of the output on the diode pump power is shown in Fig. 4 for OC transmissions of 0.3% and 1.5%. With the 0.3% OC, the laser emits an output power of 100 mW when pumped by an absorbed power of 285 mW. The slope efficiency is 40%. For the same pump power, an OC of 0.7% provided an output of 90 mW with a slope efficiency of 46%. With an OC transmission of 1.5% the slope efficiency is reduced and the output power shows a roll-over, thermally induced by pump powers exceeding 170 mW.

These observations are in good agreement with the behaviour predicted by solving the appropriate rate equations. The rate equations include thermally induced changes of several laser parameters. Thermal effects which have to be considered are the change of the upper-state lifetime by thermal quenching, and the reduction of the mode volume with increasing pump power. In addition excited state absorption (ESA) was taken into account by using a reduced value for the stimulated emission cross section [15]. Also a term for Auger upconversion [15] was added to the rate equations. The results indicated, however, that the contribution of this effect is negligibly small in this laser.

To determine the pump power dependence of the upper-state lifetime, the decay of the fluorescence intensity was measured as a function of temperature. The measured lifetimes, shown in Fig. 5, are in good agreement with the dependence predicted by the Mott-model [16], using for the radiative and nonradiative lifetime, and the activation energy the values $\tau_R = 67$ μs, $\tau_{NR} = 2.7 \times 10^{-13}$ s and $\Delta E = 4626$ cm^{-1}, respectively. With the calculated temperature distribution we estimated a pump-power-dependent average lifetime of the upper laser level within the crystal's active volume. These values (of 60 to 20 μs for pump powers in the range of 50 to 400 mW) were used to solve the rate equations.

To analyze the spectral behavior of this laser, we solved the electric-field equations for the three-mirror boundary-conditions. The result of this calculation can be illustrated by the reflectivity of the cavity (formed by the uncoated crystal surface and the output coupler), which act like an antiresonant Fabry-Perot interferometer [17]. An example for the calculated effective reflectivity of this Fabry-Perot is plotted in Fig. 6 for an output coupler with

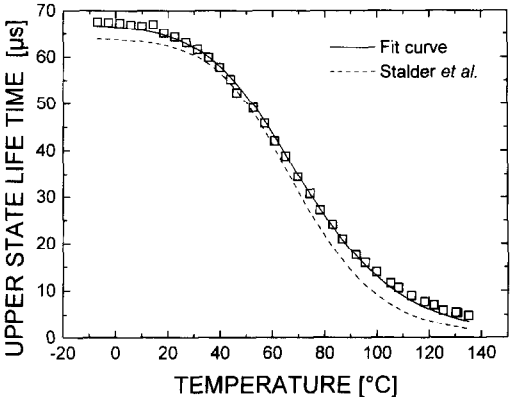

Fig. 5. Fluorescence lifetime of the upper laser level as function of crystal temperature. The dotted curves represent the dependence, calculated using the values for the radiative and nonradiative lifetime and activation energy, published by Stalder et al. [15], the solid curve shows the fit (based on the Mott model) to our experimental results.

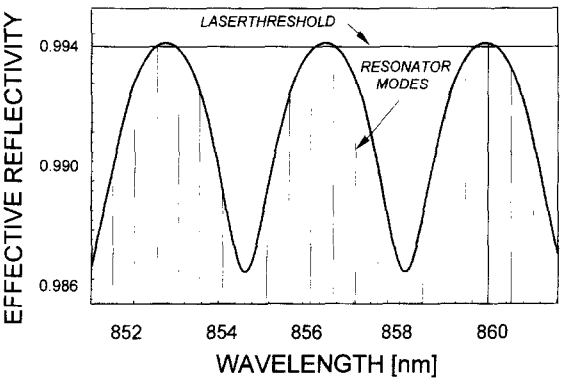

Fig. 6. Effective reflectivity calculated for the resonator which consists of the uncoated crystal surface and a 1%-output coupler, seperated by an air gap of 90 μm.

a reflectivity of 99% at a distance L_2 of 90 μm. This large value of L_2 was choosen only for illustrating in Fig. 6 more clearly the variation of the reflectivity for neighbouring laser modes.

Due to the relatively flat maxima the reflectivity for the mode at the center exceeds the reflectivity for the next modes by only a small amount (which is e.g. 0.5% for $L_2 = 10$ μm). Because of this small difference in reflectivity the threshold power is not very different for neighbouring modes. This limits the output power for single-frequency operation to 5 mW. Higher single-frequency output power could be expected, however, for an optimised combination of the reflectivities of the crystal surface (which is so far uncoated) and the outcoupling mirror.

Besides the laser system described so far, a second short cavity laser has been investigated. This laser used a grating–mirror combination in Littman-Metcalf configuration as external frequency-selective resonator [18]. The laser generated tunable single-frequency radiation within the whole gain region of the Cr:LiSAF crystal.

The scheme of the external grating resonator has been used in the past in combination with other conventional resonators [19,20]. Our investigations show that it is also of advantage for the frequency control of semi-monolithic short cavity lasers. A schematic diagram of such a laser is shown in Fig. 7. The short cavity laser is formed by the HR-coated surface of the 500 μm long Cr:LiSAF crystal and a 1.5% OC mirror. The resonator internal surface of the laser crystal is AR-coated. The external, highly dispersive resonator consists of the 1.5% OC, a grating with an angle of incidence of 77°, and a high reflective mirror. The holographic grating (1800 grooves/mm) reflected 15% in zero order and 70% in first order. The light in zero order was used for output coupling, the light in first order for frequency selective feedback. A spherical lens ($f = 40$ mm) mode-matches the two resonators. Due to the wide FSR of the short laser cavity of 215 GHz the relatively low

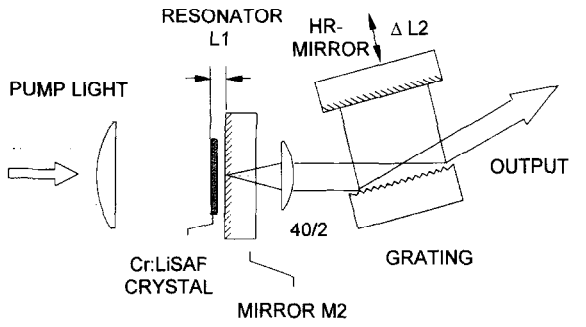

Fig. 7. Experimental setup of the Cr:LiSAF laser with an external frequency-selective grating resonator.

spectral selectivity of the grating resonator (of about 8 GHz) is fully sufficient for single-frequency operation.

When pumped with 140 mW of 670 nm diode power, this laser emitted a single-mode output power of 16 mW at a wavelength of 890 nm. The spectral linewidth was less than 1.2 MHz (measured with an optical spectrum analyzer with a free spectral range of 1.5 GHz and a finesse of 1200). A measurement of the short term frequency-stability [1] showed a linewidth of less than 600 kHz in 16 μs. The laser was tunable within a wavelength range of 800 nm to 970 nm as shown in Fig. 8.

To keep the amount of output coupling almost constant within this wavelength range, we used three differently coated mirrors M2. Continuous tuning over more than 7 GHz without mode-hops was achieved by changing simultaneously the lengths of the short laser cavity and of the external grating resonator. Continuous tuning over a larger wavelength range is expected by an additional synchronous change of the angle of the HR-mirror.

In conclusion, we have demonstrated the operation of compact single-frequency Cr:LiSAF lasers. Further improvements of the mode selectivity, the wavelength tuning, and the output power – which are in progress at present – are based on adequate solutions of the electrical field equations for the coupled cavities and on analyzing pump power dependent thermal effects (like the change of the refractive index and the shape of the laser crystal) and their influence on the laser cavity. Because of the broad operating range, the narrow linewidth and the tunability, these diode-pumped lasers should be useful e.g. for spectroscopy, or for the seeding of high power laser systems.

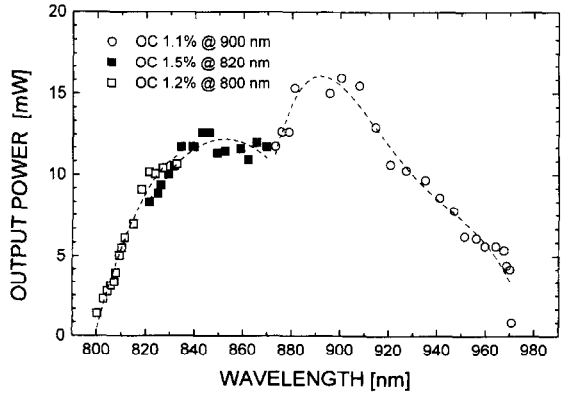

Fig. 8. Spectral dependence of the output of the Cr:LiSAF laser with external grating feedback for three differently coated mirrors M2.

Acknowledgements

We would like to thank A. Robertson for helpful discussions. This research was supported by the German Federal Ministry of Education, Science, Research and Technology.

References

[1] I. Zawischa, A.I. Ferguson, Optics Lett. 21 (1996) 45.
[2] R. Knappe, K.-J. Boller, R. Wallenstein, Optics Lett. 20 (1995) 1988.
[3] H.H. Zenzie, A. Finch, P.F. Moulton, Optics Lett. 20 (1995) 2207.
[4] J.J. Zayhowski, A. Mooradian, Optics Lett. 14 (1989) 24.
[5] P. Laporta, S. Taccheo, S. Longhi, O. Svelto, G. Sacchi, Optics Lett. 18 (1993) 1232.
[6] P. Robrish, Optics Lett. 19 (1994) 813.
[7] Q. Zhang, G.J. Dixon, B.H.T. Chai, P.N. Kean, Optics Lett. 17 (1992) 43.
[8] J.M. Sutherland, S. Ruan, R. Mellish, P.M.W. French, J.R. Taylor, Optics Comm. 113 (1995) 458.
[9] D. Findlay, R.A. Clay, Phys. Lett. 20 (1966) 277.
[10] J.Y. Yang, Uniphase APT Inc., private communication.
[11] N. MacKinnon, B.D. Sinclair, Optics Comm. 94 (1992) 281.
[12] MSC/NASTRAN, The MacNeal-Schwendler Corp, V68 on a SGI Power Challenge, regionales Hoch-schulrechenzentrum Kaiserslautern RHRK.
[13] H. Kogelnik, T. Li, Proc. IEEE 54 (1966) 1312.
[14] M.D. Perry, S.A. Payne, T. Ditmire, R. Beach, G.J. Quarles, W. Ignatuk, R. Olson, J. Weston, Laser Focus World, Sept. 1993.
[15] S.A. Payne, L.K. Smith, R.J. Beach, B.H.T. Chai, J.H. Tassano, L.D. DeLoach, W.L. Kway, R.W. Solarz, W.F. Krupke, Appl. Optics 33 (1994) 5526, and references therein.
[16] M. Stalder, M. Bass, B.H.T. Chai, J. Opt. Soc. Am. B 9 (1992) 2271.
[17] C. Pedersen, P.L. Hansen, T. Skettrup, P. Buchhave, Optics Lett. 20 (1995) 1389.
[18] M.G. Littman, H.J. Metcalf, Appl. Optics 17 (1978) 2224.
[19] C.H. Vilain, J.H. Foing, P. Schanne, ASSL '95, MF4, p. 99.
[20] M. Ihara, M. Tsunekane, N. Taguchi, H. Inaba, Electron. Lett. 31 (1995) 888.